nature materials

ARTICLES

PUBLISHED ONLINE: 13 JULY 2009; CORRECTED AFTER PRINT 13 JANUARY 2010 | DOI: 10.1038/NMAT2490

A general phase-transfer protocol for metal ions and its application in nanocrystal synthesis

Jun Yang[1,2], Edward H. Sargent[3], Shana O. Kelley[2,4]* and Jackie Y. Ying[1]*

Nanocrystals prepared in organic media can be easily self-assembled into close-packed hexagonal monolayers on solvent evaporation for various applications. However, they usually rely on the use of organometallic precursors that are soluble in organic solvents. Herein we report a general protocol to transfer metal ions from an aqueous solution to an organic medium, which involves mixing the aqueous solution of metal ions with an ethanolic solution of dodecylamine (DDA), and extracting the coordinating compounds formed between the metal ions and DDA into toluene. This approach could be applied towards transferring a wide variety of transition-metal ions with an efficiency of >95%, and enables the synthesis of a variety of metallic and semiconductor nanocrystals to be carried out in an organic medium using relatively inexpensive water-soluble metal salts as starting materials. This protocol could be easily extended to synthesize a variety of heterogeneous semiconductor/noble-metal hybrids and to nanocomposites with multiple functionalities.

Nanostructured materials are of great interest owing to their size-dependent properties[1,2]. The confinement or collective oscillation of electrons in the conduction band by a nanocrystal provides a powerful means to manipulate the electronic, optical, magnetic and catalytic properties of a solid material[3–7]. Thus, nanocrystals have been critical towards studying quantum size effects, including quantized excitation[8–10], Coulomb blockade[11,12], metal–insulator transition[13,14] and superparamagnetism[15–17].

Many metal nanoparticles can now be produced with fairly good control of particle size and shape by solution-chemistry methods in polar and non-polar solvents[18–22]. However, the design and synthesis of nanostructured materials with controlled properties remain a significant challenge[23]. Herein we report a general protocol for transferring metal ions from water to an organic medium, which involves mixing an aqueous solution of metal salts with an ethanolic solution of dodecylamine (DDA), and then extracting the metal ions into an organic layer (toluene, hexane or other non-polar solvents). It was successfully applied towards the synthesis of a variety of metallic, alloy and semiconductor nanoparticles. Compared with other general approaches[24,25], this protocol allowed nanocrystals to be synthesized in an organic medium using aqueous soluble metal salts as starting materials, which are relatively inexpensive and easily obtained. It was easily extended to synthesize a large number of semiconductor/noble-metal composite nanoparticles, including the heterogeneous deposition of noble metal on semiconductor nanoparticles, and the homogeneous growth of semiconductor on noble-metal nanoparticles.

The phase transfer of metal salts from water to an organic medium is a crucial step preceding the synthesis of nanocrystals. Metal ions could not be transferred to the organic phase by direct mixing of an aqueous metal salt solution with an organic solvent containing DDA. Prolonged agitation would result only in a turbid mixture. However, the transfer of metal ions could occur using ethanol as an intermediate solvent (on the basis of the fact that water and ethanol are miscible); this would ensure the maximum contact between the metal ions and DDA. Figure 1 illustrates the complete bleaching of the aqueous phase as the metal ions were successfully transferred from water to toluene.

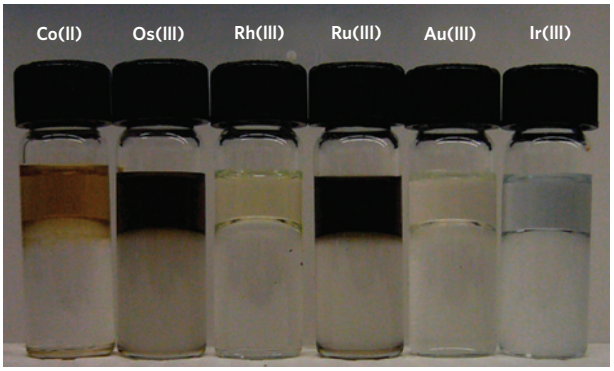

Figure 1 | Photographs showing the successful transfer of Co(II), Os(III), Rh(III), Ru(III), Au(III) and Ir(III) metal ions from the aqueous phase to toluene.

The mechanism of this protocol was different from an early transfer method for gold ions pioneered by Brust *et al.*, whereby the gold ions from an aqueous solution were directly transferred to a hydrocarbon phase (toluene) on the basis of an electrostatic interaction with tetraoctylammonium bromide[26]. A metal complex between the metal ions and DDA was speculated to have formed in the process, which could be more easily extracted by toluene. This was verified by the Fourier-transform infrared (FTIR) spectra of the compounds recovered from the organic layer after phase transfer (Fig. 2). Compared with pure DDA, differences were observed in the N–C and N–H stretching regions, demonstrating that DDA was bound to the metal ions by its NH_2 group. The X-ray photoelectron spectroscopy (XPS) analyses of N 1*s* spectra of pure DDA and several types of metal-ion/DDA complex indicated that metal ions coordinated with DDA through sharing the electron pair of the $–NH_2$ group. The electron-donating effect from $–NH_2$ to metal ions resulted in an appreciable shift of

[1]Institute of Bioengineering and Nanotechnology, 31 Biopolis Way, The Nanos, Singapore 138669, Singapore, [2]Department of Pharmaceutical Sciences, Leslie Dan Faculty of Pharmacy; [3]Department of Electrical and Computer Engineering, Faculty of Engineering; [4]Department of Biochemistry, Faculty of Medicine, University of Toronto, Toronto, Ontario M5S 3G4, Canada. *e-mail: shana.kelley@utoronto.ca; jyying@ibn.a-star.edu.sg.

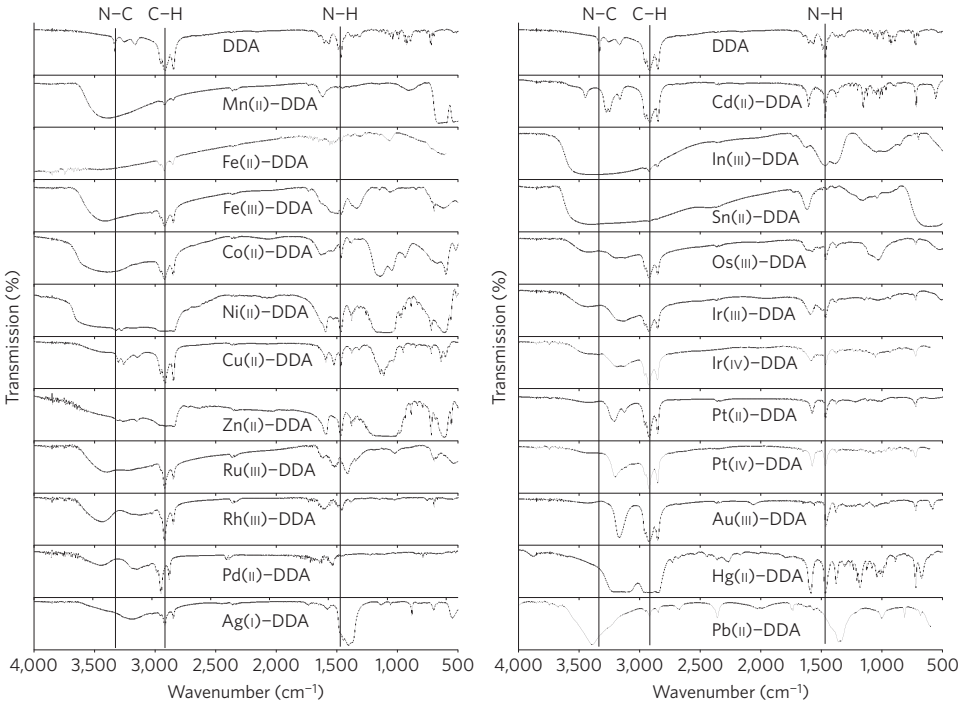

Figure 2 | FTIR spectra of pure DDA and metal-ion/DDA complexes.

the N 1*s* binding energy to a higher value (see Supplementary Fig. S1). After coordinating with metal ions, the non-polar tail of the DDA enabled the compounds to dissolve easily in non-polar organic solvents, such as toluene or hexane. The transfer efficiency (TE) and the distribution ratio (DR) were calculated using the following equations:

$$\mathrm{TE}(\%) = 100([M^{n+}]_\mathrm{i} - [M^{n+}]_\mathrm{f})/[M^{n+}]_i$$

$$\mathrm{DR} = \mathrm{TE}/(100 - \mathrm{TE})$$

where $[M^{n+}]_\mathrm{i}$ and $[M^{n+}]_\mathrm{f}$ were the initial and final metal ion concentrations in the aqueous phase, respectively. Analyses by inductively coupled plasma atomic emission spectrophotometry indicated that the phase transfer efficiencies for a wide variety of metal ions were higher than 95% (see Supplementary Table S1).

This phase-transfer protocol possessed the following advantages: (1) good ion uptake by the complexing agent, enabling fast binding with the metal ion, (2) high stability against hydrolysis, (3) selective ion complexation of heavy metals, along with no affinity for alkali or alkaline earth ions that are usually present in high concentrations in water and soil, (4) sufficiently high binding strength for the metal ions to be extracted and (5) preference of the metal complex derived for the organic phase over the aqueous phase, which would be of interest for applications in environmental remediation, such as the extraction of heavy metals from water and soil[27]. Here, we have focused on the application of this protocol in the nanocrystalline synthesis of noble metals, semiconductors and their hybrids.

Noble-metal nanoparticles could be synthesized in toluene on the addition of a reducing agent ($NaBH_4$, hexadecanediol (HDD), or tetrabutylammonium borohydride (TBAB), see Supplementary Information, Part SII) and agitation. The organic phase would change colour (for example, from yellow to red for gold) within a few minutes, indicating the successful reduction. Figure 3(1)–(4) show the transmission electron microscopy (TEM) images of nanocrystalline samples of Ag, Au, Pd and Pt, respectively. This approach has also been shown to yield nearly monodisperse metal nanoparticles of Ir, Os, Rh and Ru (see Supplementary Fig. S2). The diameters of the nanoparticles could be conveniently controlled by using different reducing agents or starting metal ions with different valencies (see Supplementary Table S2). Powder X-ray diffraction (XRD) patterns (Fig. 4a) demonstrated the successful synthesis of face-centred cubic (fcc) Rh, Pd, Ag, Ir, Pt and Au nanocrystals, and hexagonal Ru and Os nanocrystals[28]. Unlike the spherical morphology of other noble metals, Pd nanoparticles were mostly worm-like (Fig. 3(3)). This could have resulted from the existence of preferential particle growth directions, probably caused by the anisotropic adsorption of DDA on the surface of the growing Pd nanoparticles, and determined by the structure of the precursor complex formed between $PdCl_2$ and DDA.

Alloy and core–shell nanoparticles could be easily synthesized by co-reducing the metal ions and using the seed-mediated growth method respectively in toluene (see Supplementary Information, Part SIII and SIV). TEM images of Ag–Au, Pd–Pt, Pt–Rh and Pt–Ru alloys and core–shell Au@Ag and Pt@Ag nanoparticles with cores of different sizes are shown in Fig. 3(5)–(12). For the alloy Ag–Au system, a notable advantage was that the preparation could be carried out at high concentrations of metal precursors. This was because the synthesis of alloy nanoparticles in an organic medium avoided the formation of salts such as AgCl. The XRD patterns (Fig. 4b) show the presence of a homogeneously mixed crystal lattice, indicating the formation of alloy nanoparticles. The XRD pattern (Fig. 4b) of core–shell Au@Ag nanoparticles (12.7 nm Au as seeds) also showed a homogeneous phase because Ag and Au have quite similar lattice parameters[29]. However, for core–shell Pt@Ag nanoparticles (9.2 nm Pt as seeds), the XRD pattern showed two distinct metal phases, which could be indexed to the cubic Ag and Pt, respectively (Fig. 4b). The XPS spectra of the Pd–Pt, Pt–Rh and Pt–Ru alloys could all be deconvoluted into two pairs of doublets (see Supplementary Fig. S5). The more intense doublet (335.1 and 340.1 eV for Pd in Pd–Pt alloy) was attributed to metal in the zero-valence state[30]. The second and weaker doublet (336.3 and 341.0 eV for Pd in Pd–Pt alloy), with binding energies higher than those of the zero-valence metal, could be assigned to PdO, PtO, Rh_2O_3 and RuO_2, respectively. The XPS spectra of the Ag–Au alloy consisted of

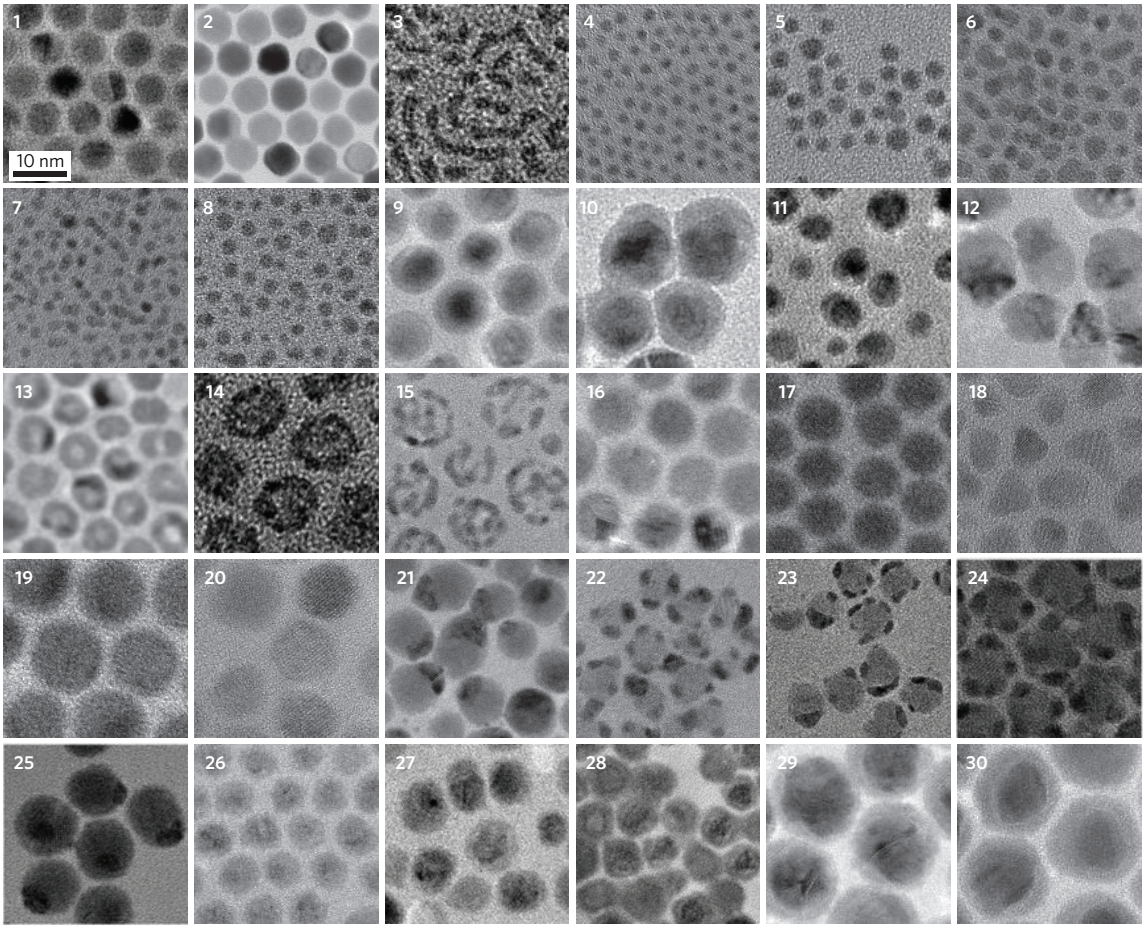

Figure 3 | TEM images of metal nanoparticles. (1) Ag derived with HDD, (2) Au, (3) worm-like Pd and (4) Pt from Pt(IV), derived with TBAB. Alloy nanoparticles of (5) Ag–Au, (6) Pd–Pt, (7) Pt–Rh and (8) Pt–Ru, synthesized by co-reduction of the metal precursors with TBAB. Core–shell nanoparticles of (9) 7.4 nm Au@Ag, (10) 12.7 nm Au@Ag, (11) 3.9 nm Pt@Ag and (12) 9.2 nm Pt@Ag, synthesized by seed-mediated growth. Core–shell nanoparticles of (13) Ag@Au and (14) Ag@Pt, synthesized by the replacement reaction. (15) Pt hollow spheres synthesized by BSPP treatment of Ag@Pt nanoparticles. (16) Ag–Pd alloy synthesized by the replacement reaction. Semiconductor nanocrystals of (17) Ag_2S, (18) CdS, (19) HgS and (20) PbS. Hybrid nanoparticles of (21) Ag_2S–Au, (22) CdS–Au, (23) CuS–Au, (24) PbS–Au, (25) Ag_2S–Ag, (26) CdS–Ag, (27) CuS–Ag and (28) PbS–Ag. Core–shell nanoparticles of Au@Ag_2S synthesized with Au/Ag_2S precursor molar ratios of (29) 1:1 and (30) 1:3. The scale of each image is identical.

doublets at 368.1 and 374.0 eV for Ag, and at 84.0 and 87.7 eV for Au; these corresponded to Ag and Au in the zero-valence state[30]. The XPS spectra of core–shell Au@Ag and Pt@Ag nanoparticles are shown in Supplementary Fig. S8. Unlike in the Pt-containing alloy nanoparticles, Pt was not oxidized in the core–shell Pt@Ag nanoparticles owing to the presence of the Ag shell.

The phase transfer of metal ions from the aqueous phase to toluene enabled us to systematically investigate the replacement reaction in an organic medium. The replacement reaction between Ag nanoparticles and $HAuCl_4$ in the aqueous phase has been extensively studied[31–33]. The resulting Au nanoshells were reported to have a hollow interior with smooth, pinhole-free surface. However, our replacement reactions between Ag nanoparticles and Au(III) and Pt(II) in an organic medium (see Supplementary Information, Part SV) have led to a number of observations different from those reported in the literature. (1) A significant shrinkage of the Ag templates occurred during the course of the replacement reaction. (2) Au or Pt atoms were deposited on the surface of the shrunken Ag templates, resulting in core–shell Ag@Au or Ag@Pt structures instead of a Au or Pt nanoshell (Fig. 3(13)–(14)). The XRD pattern (Fig. 4c) of the core–shell Ag@Au nanoparticles obtained by the replacement reaction was similar to that of core–shell Au@Ag nanoparticles (Fig. 4b), except for the broader peaks of the former (which were probably due to the finer grain size).

Core–shell Ag@Pt nanoparticles showed a broad absorption band centred at 437 nm (see Supplementary Fig. S9d), which was attributed to the surface plasmon resonance of Ag particles, because Pt has no characteristic ultraviolet–visible absorption peak. The large redshift (~37 nm) of the Ag surface plasmon band in the Ag@Pt nanoparticles relative to the Ag nanocrystalline seeds (at ~400 nm) was attributed to the presence of the Pt shell. Two distinct metal phases corresponding to Ag and Pt, respectively, were noted in the XRD pattern of core–shell Ag@Pt nanoparticles (Fig. 4c). The preservation of the optical properties of Ag cores could be due to the formation of a discontinuous Pt shell, as demonstrated by the bis(*p*-sulphonatophenyl)phenylphosphane dihydrate dipotassium salt (BSPP) treatment (see Supplementary Information, Part SV). BSPP has a strong ability to coordinate with Ag atoms or Ag(I) ions[34,35]. After agitating the mixture of aqueous solution of BSPP and Ag@Pt organosol for 12 h, the BSPP–Ag coordination compounds were formed and dissolved in an aqueous phase, leaving behind an organosol containing Pt hollow spheres. Figure 3(15) clearly illustrates the discontinuity of the resulting Pt shells. After BSPP treatment, the XRD pattern (Fig. 4c) could be indexed to the pure metallic Pt, and the Ag plasmon

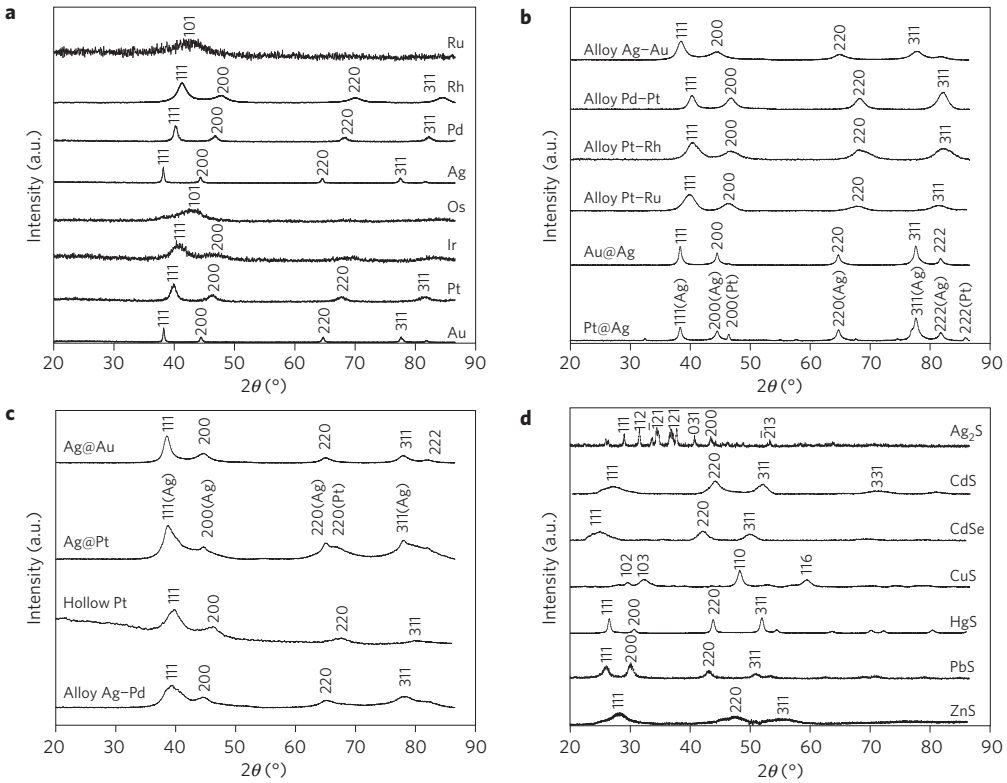

Figure 4 | XRD patterns. a–d, Spectra for noble-metal nanocrystals: hexagonal Ru and Os, and fcc Rh, Pd, Ag, Ir, Pt and Au (**a**); Ag–Au, Pd–Pt, Pt–Rh and Pt–Ru alloys, and core–shell Au@Ag and Pt@Ag (**b**); core–shell Ag@Au and Ag@Pt, hollow Pt and Ag–Pd alloy (**c**); and semiconductor nanocrystals of monoclinic Ag_2S, hexagonal CuS and fcc CdS, CdSe, HgS, PbS and ZnS (**d**).

band disappeared (see Supplementary Fig. S9d), confirming the elimination of the Ag cores from the Ag@Pt nanoparticles.

The Pt hollow spheres demonstrated superior electrocatalytic activity as compared with core–shell Ag@Pt nanoparticles in the room-temperature methanol oxidation reaction (see Supplementary Fig. S10). The discontinuous Pt shells provided for greater specific surface area, and allowed the reactants access to the internal surface of the Pt hollow nanospheres. The Pt hollow spheres could also be used to trap fluorescent dye from aqueous dye solution, and then release the dye to pure water (Fig. 5, Supplementary Information, Part SV). This unique property might be useful for drug-delivery applications.

Instead of core–shell structures, the replacement reaction between Ag nanoparticles and Pd(II) in toluene resulted in Ag–Pd alloy nanoparticles (Fig. 3(16)). High-resolution TEM (HRTEM) showed excellent atomic ordering within each particle (see Supplementary Fig. S11b), with no lattice mismatch. The uniform contrast throughout the particle further demonstrated the atomic level mixing of the metallic components. Energy-dispersive X-ray analysis (see Supplementary Fig. S11d) further illustrated the uniform distribution of Ag and Pd signals across the Ag–Pd nanoparticles. The formation of Ag–Pd alloy nanoparticles by the replacement reaction in an organic medium herein was similar to that of Ag–Au or Ag–Pd alloy nanoparticles by the replacement reaction between Ag nanoparticles and Au or Pd ions in aqueous solution[36]. The alloying process was realized by the rapid interdiffusion of metal atoms as a result of the reduced dimension of the silver templates, elevated temperature and the large number of interfacial vacancy defects generated by the replacement reaction[36].

This protocol could be further used to synthesize semiconductor nanoparticles. The metal-ion/DDA compounds were recovered from toluene in advance, and then dissolved in oleylamine. Semiconductor nanocrystals could then be obtained by carrying

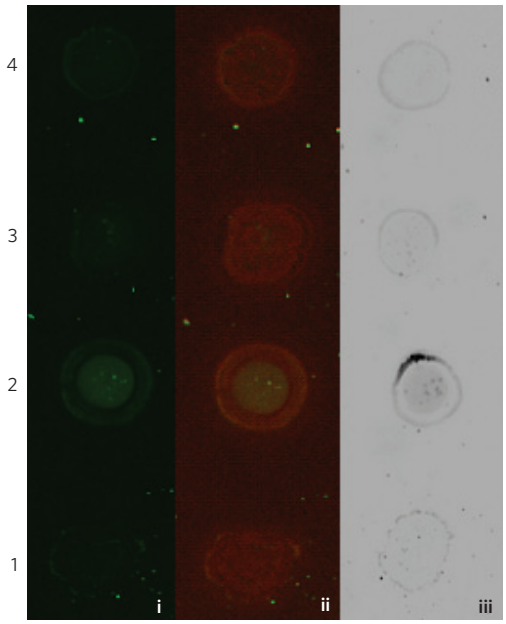

Figure 5 | Room-temperature trapping and release of SYBR Green-I by Pt hollow nanospheres. Pt hollow spheres (1) before and (2) after agitation with SYBR Green-I for 6 h, and (3) after agitation with pure water for 6 h. (4) Core–shell Ag@Pt nanoparticles after agitation with SYBR Green-I for 6 h. The same excitation wavelength was used in (i) and (iii) to detect the presence of SYBR Green-I; colour was added in (i) to highlight SYBR Green-I. Two different excitation wavelengths were used in (ii) to detect the presence of SYBR Green-I and nanoparticles, respectively. Only the hollow Pt spheres could trap fluorescent dye from aqueous dye solution, and release it again when agitated with pure water.

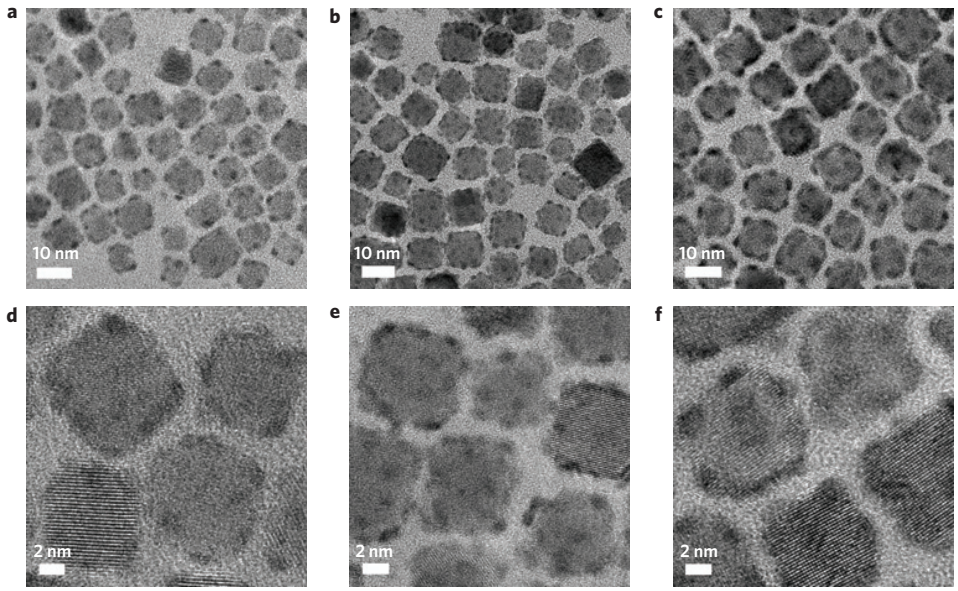

Figure 6 | PbS–Au hybrids at different Au/PbS precursor ratios. a–f, TEM images (**a–c**) and HRTEM images (**d–f**) of heterogeneous PbS–Au hybrid nanoparticles synthesized with Au/PbS precursor molar ratios of 1:4 (**a**,**d**), 1:2 (**b**,**e**) and 1:1 (**c**,**f**).

out the reaction with elemental sulphur in oleylamine at elevated temperatures (see Supplementary Information, Part SVI). These particles could be precipitated by methanol from oleylamine, and redispersed in non-polar solvents (for example, toluene, hexane and chloroform). Figure 3(17)–(20) shows the TEM images of Ag_2S, CdS, HgS and PbS nanoparticles prepared by this approach (see Supplementary Table S4 for size distributions). The successful syntheses of monoclinic Ag_2S, hexagonal CuS and fcc CdS, CdSe, HgS, PbS and ZnS nanocrystals were confirmed by XRD (Fig. 4d). It was noteworthy that for PbS, the shape could be controlled conveniently by varying the volume ratio of solvents in synthesis. Spherical, truncated cubic and cubic PbS nanocrystals were obtained with oleylamine/oleic acid volume ratios of 9:1, 3:1 and 1:3, respectively (see Supplementary Fig. S13).

To facilitate biological applications, we have developed a method to transfer the semiconductor nanocrystals synthesized in organic solvents back into the aqueous phase. Methanol was involved as a mediating solvent, but glutathione was used to replace DDA as the transfer agent and as a capping agent (see Supplementary Information, Part SVI). Supplementary Fig. S14 shows the TEM images of CdSe as-prepared and transferred from toluene. The transfer of CdSe from toluene to water was further confirmed by FTIR (see Supplementary Fig. S15). The replacement of DDA by glutathione was supported by the disappearance of the FTIR peaks at 2,850 and 2,919 cm^{-1}, which were attributed to the symmetric and asymmetric stretches of methylene groups of DDA. Identical ultraviolet–visible spectra with an excitonic absorption at 495 nm were obtained before and after the phase transfer (see Supplementary Fig. S16). A similar photoluminescent band position with a reduced intensity was obtained after the phase transfer from toluene to water, probably induced by an increase in the trapping sites during the phase transfer process[37].

An important challenge in nanocrystal synthesis is the incorporation of different materials within the same nanosystem to provide for multiple functionalities[38–47]. Nanocomposites of noble metal and semiconductor are of particular interest[38,48]. Our protocol could be easily extended to synthesize such hybrids. By ageing the mixture of semiconductor nanocrystals and noble-metal ions in toluene for 1 h, uniform semiconductor/noble-metal heterogeneous nanostructures were obtained as the dominant product. Extra reducing agent was not necessary; DDA could reduce the noble-metal ions sufficiently in the presence of semiconductor nanocrystals[45,48]. Hybrids of Ag_2S–Au, CdS–Au, CuS–Au, PbS–Au, Ag_2S–Ag, CdS–Ag, CuS–Ag and PbS–Ag were successfully prepared (Fig. 3(21)–(28)). Energy-dispersive X-ray analyses confirmed that the nanostructures were composed of semiconductors and noble metals (see Supplementary Fig. S17). Isolated noble-metal nanocrystals were not observed, indicating that noble metal nucleated preferentially on the existing semiconductor nanocrystals, rather than homogeneously, under our experimental conditions. It was noteworthy that in the absence of the semiconductor nanoparticles, the reduction of Au(III) or Ag(I) ions by DDA would require several days, suggesting that the reduction of noble-metal ions was catalysed in the presence of semiconductor nanoparticles.

The mechanism responsible for our hybrid formation might be quite similar to that for Fe_3O_4–Au hybrid nanoparticles[38]. On nucleation of the noble metal on the semiconductor surface, electron density from the semiconductor nanocrystal would be drawn to the polar semiconductor/noble-metal interface. Free electrons in the semiconductor nanocrystal might also catalyse the nucleation of noble metal, which eventually grew to form 'dots' on the semiconductor surface. The size of the noble metal on semiconductor nanocrystals could be controlled by changing the precursor molar ratio of noble metal to semiconductor. Figure 6 shows that the number and size of Au dots on each cubic PbS nanocrystal increased with increasing Au/PbS molar ratio.

Unlike the Ag_2S–Ag system, other semiconductor–Ag hybrids (CdS–Ag, CuS–Ag and PbS–Ag) had core–shell nanostructures, instead of heterogeneous hybrid nanostructures. This could be explained by the cation-exchange reactions in ionic nanocrystals[49]. Ag(I) ions exchanged with Cd(II), Cu(II) or Pb(II) on the surface of semiconductor nanocrystals, resulting in the formation of a Ag_2S shell on the shrunken semiconductor nanocrystals (see Supplementary Information, Part SVII, Scheme S1). This Ag_2S shell inhibited further exchange between Ag and Cd, Cu or Pb cations, and a core–shell semiconductor@Ag_2S structure was obtained instead of a heterogeneous hybrid. The Ag_2S shell could enhance the luminescence of CdS nanocrystals (see Supplementary Fig. S18). The maximum enhancement of the luminescence of CdS was attained at a CdS/Ag(I) molar ratio of 2:1. The small blueshift in the emission spectrum of CdS@Ag_2S relative to that of CdS nanocrystal was an indication of the shrinkage of the CdS core.

When the order of nanocrystal synthesis was reversed, that is, synthesizing Ag_2S nanocrystals in the presence of Au nanoparticles, Ag_2S would homogeneously grow on the existing Au nanoparticles, resulting in a Au@Ag_2S core–shell structure (Fig. 3(29)–(30)). The thickness of the Ag_2S shell could be controlled by varying the Au/Ag_2S precursor molar ratio. The Au@Ag_2S nanocrystals still possessed the optical properties of Au nanoparticles despite the presence of the Ag_2S shell (see Supplementary Information, Part SVII, Fig. S19). Their absorption peaks at 567, 574, 595 and 646 nm were attributed exclusively to the surface plasmon resonance of the Au cores. The large redshift of the Au surface plasmon band in the Au@Ag_2S nanocrystals relative to the pristine Au nanoparticles was due to the Ag_2S shell. The surface plasmon resonance peak of Au cores could be tuned by the Ag_2S shell thickness.

With slight modification, the method used to prepare semiconductor–metal hybrids could also be applied to derive Fe_3O_4–Ag dimers (see Supplementary Information, Part SVIII, Figs S21–S22). The Fe_3O_4 seeds were prepared following the method reported by Hyeon and co-workers[50]. The HRTEM image revealed that the crystal planes of Ag were not parallel to those of Fe_3O_4 in each heterogeneous nanostructure (inset of Supplementary Fig. S21), indicating that the growth of Ag took place in different orientations.

In summary, we have demonstrated a general protocol for transferring metal ions from water to an organic medium, which involved mixing an aqueous solution of metal ions with an ethanolic solution of DDA, and extracting the metal ions into a toluene layer. This protocol could be applied to transfer a wide variety of transition-metal ions from water to toluene with an efficiency of >95%. It led to the successful synthesis of a wide range of metallic, alloy, semiconductor and semiconductor–metal hybrid nanoparticles, and heterogeneous Fe_3O_4–Ag dimers. Thus, this approach represents a simple and flexible route for fabricating nanostructured materials with novel structures and multiple functionalities.

Methods

Phase transfer of metal ions from water to toluene. In a typical experiment, 50 ml of 1 mM aqueous metal salt solution (Mn(II), Fe(II), Fe(III), Co(II), Ni(II), Cu(II), Zn(II), Ru(III), Rh(III), Pd(II), Ag(I), Cd(II), In(III), Sn(II), Os(III), Ir(III), Ir(IV), Pt(II), Pt(IV), Au(III), Hg(II) or Pb(II)) was mixed with 50 ml of ethanol containing 1 ml of DDA. After 3 min of stirring, 50 ml of toluene was added, and stirring was continued for 1 min. Phase transfer of metal ions from water to toluene would then occur quickly and completely, as evident by the complete colour bleaching of the aqueous phase. Assuming complete transfer of the ions from water, the metal ion concentration in toluene would be 1 mM. The metal ions in toluene were separated from the aqueous phase, and kept for further experiments. The aqueous phase remaining was analysed by inductively coupled plasma atomic emission spectrophotometry to determine the transfer efficiency (see Supplementary Table S1).

Synthesis of noble-metal nanoparticles. We chose noble metals as an example to demonstrate the extension of this transfer protocol to nanocrystal synthesis. At 100 °C, 1 ml of 100 mM toluene solution of HDD, TBAB or aqueous $NaBH_4$ was added to 20 ml of the toluene solution of noble-metal salt (Ru(III), Rh(III), Pd(II), Ag(I), Os(III), Ir(III), Pt(II), Pt(IV) or Au(III)), and the mixture was agitated for several minutes. The noble-metal colloids thus obtained were highly stable, with no sign of agglomeration even after weeks of storage. The low-magnification TEM images and size distributions (summarized in Supplementary Table S2) indicated that the large quantity of nanocrystals achieved with this protocol had a narrow size distribution. The synthesis was easily scaled up by increasing the volumes of the metal ion aqueous solution, the DDA ethanolic solution and toluene proportionately.

Received 18 September 2008; accepted 22 May 2009; published online 13 July 2009; corrected online 13 January 2010

References

1. Ferrando, R., Jellinek, J. & Johnston, R. L. Nanoalloys: From theory to applications of alloy clusters and nanoparticles. *Chem. Rev.* **108,** 845–910 (2008).
2. Murray, R. W. Nanoelectrochemistry: Metal nanoparticles, nanoelectrodes, and nanopores. *Chem. Rev.* **108,** 2688–2720 (2008).
3. Xia, Y., Xiong, Y., Lim, B. & Skrabalak, S. E. Shape-controlled synthesis of metal nanocrystals: Simple chemistry meets complex physics. *Angew. Chem. Int. Ed.* **48,** 60–103 (2009).
4. Zhang, J., Sasaki, K., Sutter, E. & Adzic, R. R. Stabilization of platinum oxygen-reduction electrocatalysts using gold clusters. *Science* **315,** 220–222 (2007).
5. Watanabe, K., Menzel, D., Nilius, N. & Freund, H.-J. Photochemistry on metal nanoparticles. *Chem. Rev.* **106,** 4301–4320 (2006).
6. Bruda, C., Chen, X., Narayanan, R. & El-Sayed, M. A. Chemistry and properties of nanocrystals of different shapes. *Chem. Rev.* **105,** 1025–1102 (2005).
7. Daniel, M.-C. & Astruc, D. Gold nanoparticles: Assembly, supramolecular chemistry, quantum-size-related properties, and applications toward biology, catalysis, and nanotechnology. *Chem. Rev.* **104,** 293–346 (2004).
8. Brus, L. Noble metal nanoparticles: Plasmon electron transfer photochemistry and single-molecule Raman spectroscopy. *Acc. Chem. Res.* **41,** 1742–1749 (2008).
9. Murray, C. B., Kagan, C. R. & Bawendi, M. G. Synthesis and characterization of monodisperse nanocrystals and close-packed nanocrystal assemblies. *Annu. Rev. Mater. Sci.* **30,** 545–610 (2000).
10. Alivisatos, A. P. Semiconductor clusters, nanocrystals, and quantum dots. *Science* **271,** 933–937 (1996).
11. Kuemmeth, F., Bolotin, K. I., Shi, S. & Ralph, D. C. Measurement of discrete energy-level spectra in individual chemically synthesized gold nanoparticles. *Nano Lett.* **8,** 4506–4512 (2008).
12. Maheshwari, V., Kane, J. & Saraf, R. F. Self-assembly of a micrometres-long one-dimensional network of cemented Au nanoparticles. *Adv. Mater.* **20,** 284–287 (2008).
13. Markovich, G., Collier, C. P. & Heath, J. R. Reversible metal–insulator transition in ordered metal nanocrystal monolayers observed by impedance spectroscopy. *Phys. Rev. Lett.* **80,** 3807–3810 (1998).
14. Collier, C. P., Saykally, R. J., Shiang, J. J., Henrichs, S. E. & Heath, J. R. Reversible tuning of silver quantum dot monolayers through the metal–insulator transition. *Science* **277,** 1978–1981 (1997).
15. Laurent, S. *et al.* Magnetic iron oxide nanoparticles: Synthesis, stabilization, vectorization, physicochemical characterizations, and biological applications. *Chem. Rev.* **108,** 2064–2110 (2008).
16. Jeong, U., Teng, X., Wang, Y., Yang, H. & Xia, Y. Superparamagnetic colloids: Controlled synthesis and niche applications. *Adv. Mater.* **19,** 33–60 (2007).
17. Sun, S. Recent advances in chemical synthesis, self-assembly, and applications of FePt nanoparticles. *Adv. Mater.* **18,** 393–403 (2006).
18. Caswell, K. K., Bender, C. M. & Murphy, C. J. Seedless, surfactantless wet chemical synthesis of silver nanowires. *Nano Lett.* **3,** 667–669 (2003).
19. Kim, F., Song, J. H. & Yang, P. Photochemical synthesis of gold nanorods. *J. Am. Chem. Soc.* **124,** 14316–14317 (2002).
20. Sun, Y. & Xia, Y. Shape-controlled synthesis of gold and silver nanoparticles. *Science* **298,** 2176–2179 (2002).
21. Shankar, S. S. *et al.* Biological synthesis of triangular gold nanoprisms. *Nature Mater.* **3,** 482–488 (2004).
22. Jin, R. *et al.* Photoinduced conversion of silver nanospheres to nanoprisms. *Science* **294,** 1901–1903 (2001).
23. Dahl, J. A., Maddux, B. L. S. & Hutchison, J. E. Toward greener nanosynthesis. *Chem. Rev.* **107,** 2228–2269 (2007).
24. Wang, X., Zhuang, J., Peng, Q. & Li, Y. A general strategy for nanocrystal synthesis. *Nature* **437,** 121–124 (2005).
25. Cushing, B., Kolesnichenko, V. L. & O'Connor, C. J. Recent advances in the liquid-phase synthesis of inorganic nanoparticles. *Chem. Rev.* **104,** 3893–3946 (2004).
26. Brust, M., Walker, M., Bethell, D., Schiffrin, D. J. & Whyman, R. Synthesis of thiol-derivatized gold nanoparticles in a two-phase liquid–liquid system. *J. Chem. Soc. Chem. Commun.* **7,** 801–802 (1994).
27. Roundhill, D. M. (ed.) *Extraction of Metals from Soils and Waters* (Kluwer–Academic/Plenum, 2001).
28. McClune, W. F. (ed.) *Powder Diffraction File Alphabetical Index Inorganic Phase* (JCPDS, 1980).
29. Link, S., Wang, Z. L. & El-Sayed, M. A. Alloy formation of gold-silver nanoparticles and the dependence of plasmon absorption on their composition. *J. Phys. Chem. B* **103,** 3529–3533 (1999).
30. Wagner, C. D. *et al. NIST Standard Reference Database 20*, version 3.2 (web version).
31. Sun, Y., Mayers, B. & Xia, Y. Template-engaged replacement reaction: A one-step approach to the large-scale synthesis of metal nanostructures with hollow interiors. *Nano Lett.* **2,** 481–485 (2002).
32. Sun, Y. & Xia, Y. Multiple-walled nanotubes made of metals. *Adv. Mater.* **16,** 264–268 (2004).
33. Sun, Y. & Xia, Y. Mechanistic study on the replacement reaction between silver nanostructures and chloroauric acid in aqueous medium. *J. Am. Chem. Soc.* **126,** 3892–3901 (2004).

34. Yang, J., Lee, J. Y., Too, H. P. & Valiyaveettil, S. A bis(*p*-sulfonatophenyl)phenylphosphine-based synthesis of hollow Pt nanospheres. *J. Phys. Chem. B* **110,** 125–129 (2006).
35. Tan, Y.-N., Yang, J., Lee, J. Y. & Wang, D. I. C. Mechanistic study on the bis(*p*-sulfonatophenyl)phenylphosphine synthesis of monometallic Pt hollow nanoboxes using Ag^{+}–Pt core–shell nanocubes as sacrificial templates. *J. Phys. Chem. C* **111,** 14084–14090 (2007).
36. Zhang, Q., Lee, J. Y., Yang, J., Boothroyd, C. & Zhang, J. Size and composition tunable Ag–Au alloy nanoparticles by replacement reactions. *Nanotechnology* **18,** 245605 (2007).
37. Aldana, J., Wang, A. & Peng, X. Photochemical instability of CdSe nanocrystals coated by hydrophilic thiols. *J. Am. Chem. Soc.* **123,** 8844–8850 (2001).
38. Mokari, T., Rothenberg, E., Popov, I., Costi, R. & Banin, U. Selective growth of metal tips onto semiconductor quantum rods and tetrapods. *Science* **304,** 1787–1790 (2004).
39. Pacholski, C., Kornowski, A. & Weller, H. Nanomaterials: Site-specific photodeposition of silver on ZnO nanorods. *Angew. Chem. Int. Ed.* **43,** 4774–4777 (2004).
40. Milliron, D. J. *et al.* Colloidal nanocrystal heterostructures with linear and branched topology. *Nature* **430,** 190–195 (2004).
41. Gu, H., Zheng, R., Zhang, X. & Xu, B. Facile one-pot synthesis of bifunctional heterodimers of nanoparticles: A conjugate of quantum dot and magnetic nanoparticles. *J. Am. Chem. Soc.* **126,** 5664–5665 (2004).
42. Yu, H. *et al.* Dumbbell-like bifunctional Au–Fe_3O_4 nanoparticles. *Nano Lett.* **5,** 379–382 (2005).
43. Li, Y., Zhang, Q., Nurmikko, A. V. & Sun, S. Enhanced magnetooptical response in dumbbell-like Ag–$CoFe_2O_4$ nanoparticle pairs. *Nano Lett.* **5,** 1689–1692 (2005).
44. Yi, D. K. *et al.* Silica-coated nanocomposites of magnetic nanoparticles and quantum dots. *J. Am. Chem. Soc.* **127,** 4990–4991 (2005).
45. Shi, W. *et al.* A general approach to binary and ternary hybrid nanocrystals. *Nano Lett.* **6,** 875–881 (2006).
46. Selvan, S. T., Patra, P. K., Ang, C. Y. & Ying, J. Y. Synthesis of silica-coated semiconductor and magnetic quantum dots and their use in the imaging of live cells. *Angew. Chem. Int. Ed.* **46,** 2448–2452 (2007).
47. Jiang, J. *et al.* Bifunctional Fe_3O_4–Ag heterodimer nanoparticles for two-photon fluorescence imaging and magnetic manipulation. *Adv. Mater.* **20,** 4403–4407 (2008).
48. Mokari, T., Sztrum, C. G., Salant, A., Rabani, E. & Banin, U. Formation of asymmetric one-sided metal-tipped semiconductor nanocrystal dots and rods. *Nature Mater.* **4,** 855–863 (2005).
49. Son, D. H., Hughes, S. M., Yin, Y. & Alivisatos, A. P. Cation exchange reactions in ionic nanocrystals. *Science* **306,** 1009–1012 (2004).
50. Park, J. *et al.* Ultra-large-scale syntheses of monodisperse nanocrystals. *Nature Mater.* **3,** 891–895 (2004).

Acknowledgements

We thank Y. K. Kuan of the Institute of Bioengineering and Nanotechnology, Singapore, for his assistance in characterizing the Pt hollow nanospheres. J.Y. and J.Y.Y. acknowledge the support by the Institute of Bioengineering and Nanotechnology (Biomedical Research Council, Agency for Science, Technology and Research, Singapore). J.Y., E.H.S. and S.O.K. acknowledge the University of Toronto, the US Air Force (MURI grant to S.O.K.) and the NIH (CA1222878-01A2). E.H.S. also acknowledges the Canada Research Chairs, the Canada Foundation for Innovation, and the Natural Sciences and Engineering Council of Canada.

Additional information

Supplementary information accompanies this paper on www.nature.com/naturematerials. Reprints and permissions information is available online at http://npg.nature.com/reprintsandpermissions. Correspondence and requests for materials should be addressed to S.O.K. or J.Y.Y.

CORRIGENDUM

A general phase-transfer protocol for metal ions and its application in nanocrystal synthesis

Jun Yang and Jackie Y. Ying

Nature Materials **8,** 683–689 (2009); published online 13 July 2009; corrected after print 13 January 2010.

The originally listed authors of the above Article wish to add a further two names as co-authors. The full author list, affiliations and acknowledgements should have been:

Jun Yang[1,2], Edward H. Sargent[3], Shana O. Kelley[2,4]* and Jackie Y. Ying[1]*

[1]Institute of Bioengineering and Nanotechnology, 31 Biopolis Way, The Nanos, Singapore 138669, Singapore. [2]Department of Pharmaceutical Sciences, Leslie Dan Faculty of Pharmacy, [3]Department of Electrical and Computer Engineering, Faculty of Engineering, [4]Department of Biochemistry, Faculty of Medicine, University of Toronto, Toronto, Ontario, Canada M5S 3G4.
*e-mail: jyying@ibn.a-star.edu.sg; shana.kelley@utoronto.ca

Acknowledgements
We thank Y. K. Kuan of the Institute of Bioengineering and Nanotechnology, Singapore, for his assistance in characterizing the Pt hollow nanospheres. J.Y. and J.Y.Y. acknowledge the support by the Institute of Bioengineering and Nanotechnology (Biomedical Research Council, Agency for Science, Technology and Research, Singapore). J.Y., E.H.S. and S.O.K. acknowledge the University of Toronto, the US Air Force (MURI grant to S.O.K.) and the NIH (CA1222878-01A2). E.H.S. also acknowledges the Canada Research Chairs, the Canada Foundation for Innovation, and the Natural Sciences and Engineering Council of Canada.

These corrections have now been made to the HTML and PDF versions of the Article.